Inorganic Chemistry
Article

Inorg. Chem. **2009**, *48*, 7201–7210 **7201**
DOI: 10.1021/ic9004467

Speciation and Structural Study of U(IV) and -(VI) in Perchloric and Nitric Acid Solutions

Atsushi Ikeda-Ohno,*,†,‡ Christoph Hennig,*,† Satoru Tsushima,† Andreas C. Scheinost,† Gert Bernhard,† and Tsuyoshi Yaita‡

†*Institute of Radiochemistry, Forschungszentrum Dresden-Rossendorf, P.O. Box 510119, 01314 Dresden, Germany, and* ‡*Synchrotron Radiation Research Center (SPring-8), Japan Atomic Energy Agency, Kouto 1-1-1, Sayo-cho, Sayo-gun, 679-5148 Hyogo-ken, Japan*

Received March 6, 2009

In order to elucidate the uranium solution chemistry at the high HNO_3 concentrations typically employed for the reprocessing of spent nuclear fuels, speciation and complex structures of U^{IV} and U^{VI} are studied in aqueous HNO_3 solutions, as well as in $HClO_4$ solutions, by means of UV−visible−near-infrared and X-ray absorption spectroscopies and density functional theory calculations. In 1.0 M $HClO_4$, U^{IV} exists as a spherical cation of U^{4+}, which is surrounded by 9−10 water molecules in the primary coordination sphere, while it forms a colloidal hydrous oxide, $U^{IV}O_2 \cdot nH_2O$, at a lower acidic concentration of 0.1 M $HClO_4$. U^{VI} exists as a transdioxo uranyl cation, UO_2^{2+}, and forms a 5-fold pure hydrate complex of $[U^{VI}O_2(H_2O)_5]^{2+}$ in 1.0 M $HClO_4$. With increasing HNO_3 concentration, the water molecules of the U^{IV} and U^{VI} hydrate complexes are successively replaced by planar bidentate coordinating nitrate ions (NO_3^-), forming dominant species of $[U^{IV}(H_2O)_x(NO_3)_5]^-$ in 9.0 M HNO_3 and $[U^{VI}O_2(NO_3)_3]^-$ in 14.5 M HNO_3, respectively. The present multitechnique approach also suggests the formation of two intermediate U^{VI} species, a 5-fold mononitrato complex ($[U^{VI}O_2(H_2O)_3(\eta_2\text{-}NO_3)]^+$) and a 6-fold dinitrato complex ($[U^{VI}O_2(H_2O)_2(\eta_2\text{-}NO_3)_2]^0$), involving an increase in the total coordination number on the uranyl(VI) equatorial plane from 5 to 6 with increasing HNO_3 concentration. The presence of unidentate coordinate nitrato complexes or tetranitrato U^{VI} complexes is less probable in the present HNO_3 system.

Introduction

The complexes of uranium (U) with nitrate ions (NO_3^-) are some of the most fundamental species in the reprocessing of spent nuclear fuels. In the PUREX process,[1] which is the most widely employed process in commercial reprocessing plants, spent nuclear fuels are dissolved and fissile U and plutonium (Pu) are separated from other actinides (An) and fission products in an aqueous nitric acid (HNO_3) medium. The chemical behavior of nuclides in the process, such as solubility or separability, strongly depends on their chemical forms. Therefore, detailed and reliable information on the chemical species of U with NO_3^- in solution is indispensable not only for maintaining and optimizing the currently operating process but also for developing more efficient methods. For this reason, U speciation in nitrate solutions has long been an important research topic for reprocessing technology and has been extensively investigated by thermodynamic,[2] spectroscopic,[3−14] and theoretical methods[15−17] for the past several decades.

Aqueous uranium nitrato complexes are the most primary species in the current PUREX-based reprocessing process

*To whom correspondence should be addressed. E-mail: a.ikeda-ohno@spring8.or.jp (A.I.-O.), hennig@esrf.fr (C.H.).

(1) (a) Long, J. T. In *Engineering For Nuclear Fuel Reprocessing*; American Nuclear Society: La Grange Park, IL, 1978.(b) Benedict, M.; Pigford, T. H.; Levi, H. W. In *Nuclear Chemical Engineering*, 2nd ed.; McGraw-Hill: New York, 1981.
(2) Grenthe, I.; Fuger, J.; Konings, R. J. M.; Lemire, R. J.; Muller, A. B.; Nguyen-Trung, C.; Wanner, H. In *Chemical Thermodynamics of Uranium*; Wanner, H., Forest, I., Eds.; OECD-NEA: Paris, 1991 (2003 updated).
(3) (a) Ermolaev, N. P.; Krot, N. N. *Radiokhimiya* **1962**, *4*, 678–685. (b) McKay, H. A. C.; Woodhead, J. L. *J. Chem. Soc.* **1964**, 717–723. (c) Rykov, A. G.; Vasil'ev, V. Y. *Radiokhimiya* **1970**, *12*, 717–727.
(4) du Preez, J. G. H.; Van Vuuren, C. P. J. *J. Inorg. Nucl. Chem.* **1974**, *36*, 81–85.
(5) Betts, R. H.; Michels, R. K. *J. Chem. Soc.* **1949**, S286–S294.
(6) Kaplan, L.; Hildebrandt, R. A.; Ader, M. *J. Inorg. Nucl. Chem.* **1956**, *2*, 151–163.
(7) Volod'ko, L. V.; Sevchenko, A. N.; Turetskaya, E. A. *J. Appl. Spec.* **1967**, *6*, 250–252.
(8) Brooker, M. H.; Huang, C.-H.; Sylwestrowicz, J. *J. Inorg. Nucl. Chem.* **1980**, *42*, 1431–1440.
(9) Couston, L.; Pouyat, D.; Moulin, C.; Decambox, P. *Appl. Spectrosc.* **1995**, *49*, 349–353.
(10) Moulin, C.; Decambox, P.; Mauchien, P.; Pouyat, D.; Couston, L. *Anal. Chem.* **1996**, *68*, 3204–3209.
(11) Fedorov, Y. S.; Zilberman, B. Y. *Radiochem.* **2000**, *42*, 242–246.
(12) Houwer, S. D.; Görller-Walrand, C. *J. Alloys Compd.* **2001**, *323−324*, 683–687.
(13) Servaes, K.; Hennig, C.; Billard, I.; Gaillard, C.; Binnemans, K.; Görller-Walrand, C.; van Deun, R. *Eur. J. Inorg. Chem.* **2007**, 5120–5126.
(14) Ikeda, A.; Hennig, C.; Rossberg, A.; Tsushima, S.; Scheinost, A. C.; Bernhard, G. *Anal. Chem.* **2008**, *80*, 1102–1110.
(15) de Jong, W. A.; Aprà, E.; Windus, T. L.; Nichols, J. A.; Harrison, R. J.; Gutowski, K. E.; Dixon, D. A. *J. Phys. Chem. A* **2005**, *109*, 11568–11577.
(16) Bühl, M.; Kabrede, H.; Diss, R.; Wipff, G. *J. Am. Chem. Soc.* **2006**, *128*, 6357–6368.
(17) Bühl, M.; Diss, R.; Wipff, G. *Inorg. Chem.* **2007**, *46*, 5196–5206.

Published on Web 07/02/2009

because most of the unit operations are carried out in aqueous HNO_3 media. The behavior of nuclides in the process is determined by several different factors. In particular, the structural arrangement of species, that is, complex structure, plays a key role. For instance, the extraction efficiency of metal cations with organic extractants is strongly influenced by the number of surrounding counteranions (= total charge of the complex) in the solvent extraction process. As a matter of fact, structural studies have already been performed on the aqueous nitrate species of Np and Pu, which are also major nuclides in spent nuclear fuels, using X-ray absorption spectroscopy.[18,19] However, despite its importance in the reprocessing process, no study has focused on the structural arrangement of aqueous uranium nitrate species to date.

Uranium can generally exist in tetravalent (U^{IV}) and hexavalent (U^{VI}) states in solution. The tetravalent U forms a spherical coordinating cation (U^{4+}), while the hexavalent one exists as a transdioxouranyl cation (UO_2^{2+}). This structural change between U^{IV} and U^{VI} naturally gives rise to the difference in their complexation properties. Therefore, understanding the actual behavior of U in the reprocessing process requires comparative information on U^{IV} and U^{VI}. However, regardless of the extensive precedent works mentioned above, there is no comparative study on U^{IV} and U^{VI} species in an aqueous nitrate solution. Even more importantly, most of the precedent works were carried out at low nitrate concentrations below 1 M, because thermodynamic methods, which have been well-developed and very informative for speciation study, are generally reliable only at an ionic strength (I) below ~3 M.[20] Since the actual PUREX processes involves the use of much higher HNO_3 concentrations (> 6 M), there is a substantial gap in information on uranium speciation at such a high nitrate concentration range.

In the present study, we investigate the chemical species of U^{IV} and U^{VI} in a wide HNO_3 concentration range (0−14.5 M) using UV−visible−near-infrared (NIR) and X-ray absorption spectroscopies and density functional theory (DFT) calculations, in order to elucidate their speciation at different HNO_3 concentrations, as well as their complex structure. Extended X-ray absorption fine structure (EXAFS) spectroscopy is a very powerful tool used to determine the local arrangement of dissolved species, such as interatomic distances (R) or coordination numbers (CN), directly. However, this technique provides only the information on statistically average species in a measured sample, meaning that it cannot differentiate several coexisting species in the same system. To complement this weak point of EXAFS, the structural information derived from EXAFS is comprehensively interpreted with the speciation information inferred from UV−visible absorption spectral titration and the DFT-optimized structures of individual species. The obtained results are also compared and discussed with the nitrate species of other actinides.

Experimental Section

Sample Preparation. All of the samples were prepared from $UO_2(NO_3)_2 \cdot 6H_2O$ (Lachema, Ltd.). U^{VI} samples were prepared by dissolving $UO_2(NO_3)_2 \cdot 6H_2O$ in a desired concentration of $HClO_4$ or HNO_3 (Merck KGaA). The nitrate concentration was varied from 0 to 14.5 M with a constant concentration step, giving a total sample number of 11. The U concentration in each sample was adjusted to 0.04 M. U^{IV} samples were electrochemically prepared from the corresponding U^{VI} solution ([U] = 0.05 M) by using an Autolab PGSTAT302 potentiostat/galvanostat (Metrohm/Eco Chemie B.V.) with a three-electrode system (Pt-plate working and counter electrodes and a Ag/AgCl reference electrode). Coulometric electroreduction of U^{VI} was performed at −0.3 V (vs Ag/AgCl, the potential values written hereafter always refer to Ag/AgCl) under an inert N_2 atmosphere. In the case of nitrate samples, hydrazine monohydrate (Sigma-Aldrich, Inc.) was added to the initial U^{VI} solution with a bit of an excess stoichiometric amount of U, in order to avoid the reoxidation of U^{IV} by nitrous acid (HNO_2).[21,22] The oxidation state of U before and after the electrolysis was confirmed by UV−visible−NIR absorption spectroscopy. All of the chemicals (except the uranyl compound) used in this study were reagent grade and used as supplied.

Spectroscopic Measurements. UV−visible−NIR absorption spectra were collected on a Cary 5G UV−visible−NIR spectrophotometer (Varian, Inc.) with 1.00 cm path length quartz cuvettes at ambient temperature. Cuvettes for U^{IV} samples were doubly sealed in an inert N_2 glovebox to avoid the penetration of O_2 into the samples.

EXAFS measurements were performed on the Rossendorf beamline BM20[23] at the European Synchrotron Radiation Facility under dedicated ring operating conditions (6 GeV; 180−200 mA). A Si(111) double-crystal monochromator was employed in the channel-cut mode to monochromatize a white X-ray from the synchrotron. Uranium L_{III}-edge absorption spectra were collected in the transmission mode using Ar-filled ionization chambers at ambient temperature and pressure. The energy of the measured spectra was corrected by referring to the first inflection point of yttrium foil (17 038 eV), which was measured simultaneously. The threshold energy, $E_{k=0}$, of the U L_{III} edge was defined at 17 185 eV, regardless of the oxidation state of U. The samples for EXAFS measurement were identical with those used for UV−visible−NIR absorption measurement. The U^{IV} samples for EXAFS measurement were completely sealed up in a quartz glass cuvette with a 1.00 cm optical path length by hot melting, while the U^{VI} samples were transferred to a polyethylene container (optical path length = 1.3 cm) and sealed by melting. Each sample was measured at least three times, and the spectra were averaged.

The collected spectra were analyzed according to a standard procedure[24] by using the program *WinXAS* (version 3.1).[25] Theoretical phase and amplitude functions for curve fitting were calculated using FEFF 8.20[26] on the basis of the reported crystal structures of $UO_2(H_2O)_5(ClO_4)_2$[27] and $UO_2(NO_3)_2(H_2O)_2$.[28] All of the possible single scattering (SS) and multiple scattering (MS) paths were taken into account in the curve fit procedure. The amplitude reduction factor, S_0^2, was fixed at 0.9, and the

(18) Ikeda-Ohno, A.; Hennig, C.; Rossberg, A.; Funke, H.; Scheinost, A. C.; Bernhard, G.; Yaita, T. *Inorg. Chem.* **2008**, *47*, 8294–8305.
(19) Allen, P. G.; Veirs, D. K.; Conradson, S. D.; Smith, C. A.; Marsh, S. F. *Inorg. Chem.* **1996**, *35*, 2841–2845.
(20) Laden, I. *Z. Phys. Chem.* **1941**, *A188*, 160–181.
(21) (a) Shabbir, M.; Robins, R. G. *J. Appl. Chem.* **1968**, *18*, 129–134. (b) Shabbir, M.; Robins, R. G. *J. Appl. Chem.* **1969**, *19*, 52–56.
(22) Biddle, P.; Miles, J. H. *J. Inorg. Nucl. Chem.* **1968**, *30*, 1291–1297.
(23) Matz, W.; Schell, N.; Bernhard, G.; Prokert, F.; Reich, T.; Claussner, J.; Oehme, W.; Schlenk, R.; Dienel, S.; Funke, H.; Eichhorn, F.; Betzl, M.; Pröhl, D.; Strauch, U.; Hüttig, G.; Krug, H.; Neumann, W.; Brendler, V.; Reichel, P.; Denecke, M. A.; Nitsche, H. *J. Synchrotron Radiat.* **1999**, *6*, 1076–1085.
(24) Prins, R.; Koningsberger, D. E. *X-ray Absorption: Principles, Applications, Techniques for EXAFS, SEXAFS, and XANES*; Wiley−Interscience: New York, 1988.
(25) Ressler, T. *J. Synchrotron Radiat.* **1998**, *5*, 118–122.
(26) Ankudinov, A. L.; Ravel, B.; Rehr, J. J.; Conradson, S. D. *Phys. Rev. B* **1998**, *58*, 7565–7576.
(27) Fischer, A. *Z. Anorg. Allgem. Chem.* **2003**, *629*, 1012–1016.
(28) Taylor, J. C.; Mueller, M. H. *Acta Crystallogr.* **1965**, *19*, 536–543.

shifts in the threshold energy, ΔE_0, were constrained to be the same value for all shells.

Computational Methods. DFT calculations were carried out to optimize the structure of aqueous U^{VI} nitrato complexes in the aqueous phase, as well as to compare the stability of their isomeric complexes. Geometry optimization and Gibbs energy calculations were performed in the aqueous phase at the B3LYP level using CPCM[29] with UAHF radii[30] with the program package Gaussian 03.[31] Small core effective core potentials (ECPs) were used on U, O, and N atoms with the corresponding basis sets.[32] The Gibbs energy correction to the electronic energy was calculated at the B3LYP level from the vibrational energy levels in the aqueous phase and the molecular partition functions. Wåhlin et al. have studied the water exchange reactions of the uranyl(VI) ion using various theories, such as B3LYP, MP2, CCSD(T), or minimal CASPT2.[33] They concluded that, as compared to CCSD(T) or CASPT2, B3LYP produces a 10−15 kJ/mol error in energy. Therefore, the accuracy of the calculations in this study is considered to be 10−15 kJ/mol at best.

Results and Discussion

Perchloric Acid System. The perchlorate ion (ClO_4^-) is known to be a noncomplexing ligand for An ions because of its weak coordination ability, especially in an aqueous solution.[34] Therefore, An species in the aqueous perchlorate medium are considered to be pure hydrate complexes. Since the pure hydrate complex is the most fundamental species in the aqueous solution system, the perchloric acid ($HClO_4$) system was investigated before the nitric acid system.

U^{VI}−perchlorate samples were prepared by dissolving $UO_2(NO_3)_2 \cdot 6H_2O$ in $HClO_4$. U^{IV}−perchlorate samples were obtained by electrolyzing the U^{VI} samples using a Pt working electrode. The electrochemical behavior of U^{VI} on the Pt electrode in $HClO_4$ was irreversible, producing only one cathodic peak in the cyclic voltammagram between −0.3 and +0.2 V (see Figure S1 in the Supporting Information). The electroreduction of U^{VI} in 1.0 M $HClO_4$ at −0.3 V produced a dark green solution. The UV−visible−NIR absorption spectrum of this dark green solution (Figure S2 in the Supporting Information) agrees with the reported spectrum for U^{IV}.[35] Performing the same electroreduction in a lower acidity of 0.1 M $HClO_4$, however, yielded an almost intransparent colloidal solution with a black color. This black colloidal solution is stable in the air for more than one month.

Figure 1 shows the k^3-weighted U L_{III}-edge EXAFS spectra for the prepared U^{VI} and U^{IV} samples in $HClO_4$ (left) and their corresponding Fourier transforms (FTs, right). The EXAFS spectrum of U^{IV} in 1.0 M $HClO_4$ consists of a single oscillation pattern, producing only one FT peak at $R + \Delta = 1.9$ Å, which corresponds to the oxygen atoms of water molecules ($O(H_2O)$) in the primary coordination sphere of the spherically coordinating U^{4+}. In contrast, the EXAFS oscillation pattern for the U^{VI} sample is more complicated, and its FT shows several peaks. Considering the fact that U^{VI} forms a transdioxo uranyl unit, the largest FT peak at $R + \Delta = 1.4$ Å, and the small peak at $R + \Delta = 2.9$ Å arises from the SS and MS[24] paths of the axial oxygens (O_{ax}) of the uranyl unit.[13,14,36] The second largest peak at around $R + \Delta = 1.9$ Å corresponds to the oxygen atoms of water molecules ($O_{eq}(H_2O)$) on the equatorial plane of the uranyl unit. The curve fit results for these spectra indicate that U^{4+} is surrounded by 10.5 water molecules at 2.40 Å, while U^{VI} forms the uranyl unit, UO_2^{2+}, with $R(U-O_{ax}) = 1.77$ Å and possesses 5.0 water molecules at 2.40 Å on the equatorial plane. It has been reported that the homologous tetravalent An of Th^{IV} and Np^{IV} are coordinated predominantly by 10 water molecules with $R(An-O(H_2O)) = 2.46$[37] and 2.40 Å[18] in aqueous solution, respectively. This indicates that the 10-coordinate aquo complex of $[U^{IV}(H_2O)_{10}]^{4+}$ may be a more probable species for U^{IV} than the 9- or 11-coordinate ones. U^{4+} and Np^{4+} show the same $An-O(H_2O)$ distance of 2.40 Å, implying that their aquo complexes are almost identical from the structural point of view. This result is in accordance with the reported DFT calculations,[38] where the average $An-O(H_2O)$ distances in 10-coordinate U^{4+} and Np^{4+} aquo complexes with C_{2v} symmetry were found to be nearly equal. On the other hand, bond valence sum calculation[18,39] suggests that the obtained interatomic distance of $R(U^{IV}-O(H_2O)) = 2.40$ Å is statistically appropriate for a CN of 8.8,[40] close to 9. Additionally, the EXAFS spectral comparison among Th^{IV}, U^{IV}, and Np^{IV} clearly demonstrates that the hydrate species of U^{IV} has a smaller CN than the Th^{IV} one but an almost identical CN to the Np^{IV} one (see Figure S21 in the Supporting Information). This means that, when assuming CN = 10 for the Th^{IV} hydrate species,[37] the CN for U^{IV} and Np^{IV} hydrate species should be less than 10. Furthermore, it should be noted that CN is correlated with the amplitude reduction factor, S_0^2, in the EXAFS curve fit procedure. The CN of 10.5 was calculated for the

(29) Barone, V.; Cossi, M. *J. Phys. Chem. A* **1998**, *102*, 1995–2001.
(30) Bondi, A. *J. Phys. Chem.* **1964**, *68*, 441–451.
(31) Frisch, M. J.; Trucks, G. W.; Schlegel, H. B.; Scuseria, G. E.; Robb, M. A.; Cheeseman, J. R.; Montgomery, J. A., Jr.; Vreven, T.; Kudin, K. N.; Millam, J. M.; Iyengar, S. S.; Tomasi, J.; Barone, V.; Mennucci, B.; Cossi, M.; Scalmani, G.; Rega, N.; Petersson, G. A.; Nakatsuji, H.; Hada, M.; Ehara, M.; Toyota, K.; Fukuda, R.; Hasegawa, J.; Ishida, M.; Nakajima, T.; Honda, Y.; Kitao, O.; Nakai, H.; Klene, M.; Li, X.; Knox, J. E.; Hratchian, H. P.; Cross, J. B.; Bakken, V.; Adamo, C.; Jaramillo, J.; Gomperts, R.; Stratmann, R. E.; Yazyev, O.; Austin, A. J.; Cammi, R.; Pomelli, C.; Ochterski, J. W.; Ayala, P. Y.; Morokuma, K.; Voth, G. A.; Salvador, P.; Dannenberg, J. J.; Zakrzewski, V. G.; Dapprich, S.; Daniels, A. D.; Strain, M. C.; Farkas, O.; Malick, D. K.; Rabuck, A. D.; Raghavachari, K.; Foresman, J. B.; Ortiz, J. V.; Cui, Q.; Baboul, A. G.; Clifford, S.; Cioslowski, J.; Stefanov, B. B.; Liu, G.; Liashenko, A.; Piskorz, P.; Komaromi, I.; Martin, R. L.; Fox, D. J.; Keith, T.; Al-Laham, M. A.; Peng, C. Y.; Nanayakkara, A.; Challacombe, M.; Gill, P. M. W.; Johnson, B.; Chen, W.; Wong, M. W.; Gonzalez, C.; Pople, J. A. *Gaussian 03*, revision D.01; Gaussian, Inc.: Wallingford, CT, 2004.
(32) Küchle, W.; Dolg, M.; Stoll, H.; Preuss, H. *J. Chem. Phys.* **1994**, *100*, 7535–7542.
(33) Wåhlin, P.; Danilo, C.; Vallet, V.; Réal, F.; Flament, J.-P.; Wahlgren, U. *J. Chem. Theory Comput.* **2008**, *4*, 569–577.
(34) (a) Sémon, L.; Boehme, C.; Billard, I.; Hennig, C.; Lützenkirchen, K.; Reich, T.; Rossberg, A.; Rossini, I.; Wipff, G. *ChemPhysChem* **2001**, *2*, 591–598. (b) Antonio, M. R.; Soderholm, L.; Williams, C. W.; Blaudeau, J.-P.; Bursten, B. E. *Radiochim. Acta* **2001**, *89*, 17–25.
(35) Kraus, K. A.; Nelson, F. *J. Am. Chem. Soc.* **1950**, *72*, 3901–3906.
(36) Hennig, C.; Tutschku, J.; Rossberg, A.; Bernhard, G.; Scheinost, A. C. *Inorg. Chem.* **2005**, *44*, 6655–6661.
(37) Wilson, R. E.; Skanthakumar, S.; Burns, P. C.; Soderholm, L. *Angew. Chem., Int. Ed.* **2007**, *46*, 8043–8045.
(38) Tsushima, S.; Yang, T. X. *Chem. Phys. Lett.* **2005**, *401*, 68–71.
(39) Brown, I. D. *Chem. Soc. Rev.* **1978**, *7*, 359–376.
(40) Calculation was performed by assuming a bond distance parameter, $R_{ij}(U^{IV})$, of 2.126 Å and an empirical parameter, B, of 0.37: Zachariasen, W. H. *J. Less-Common Met.* **1978**, *62*, 1–7.

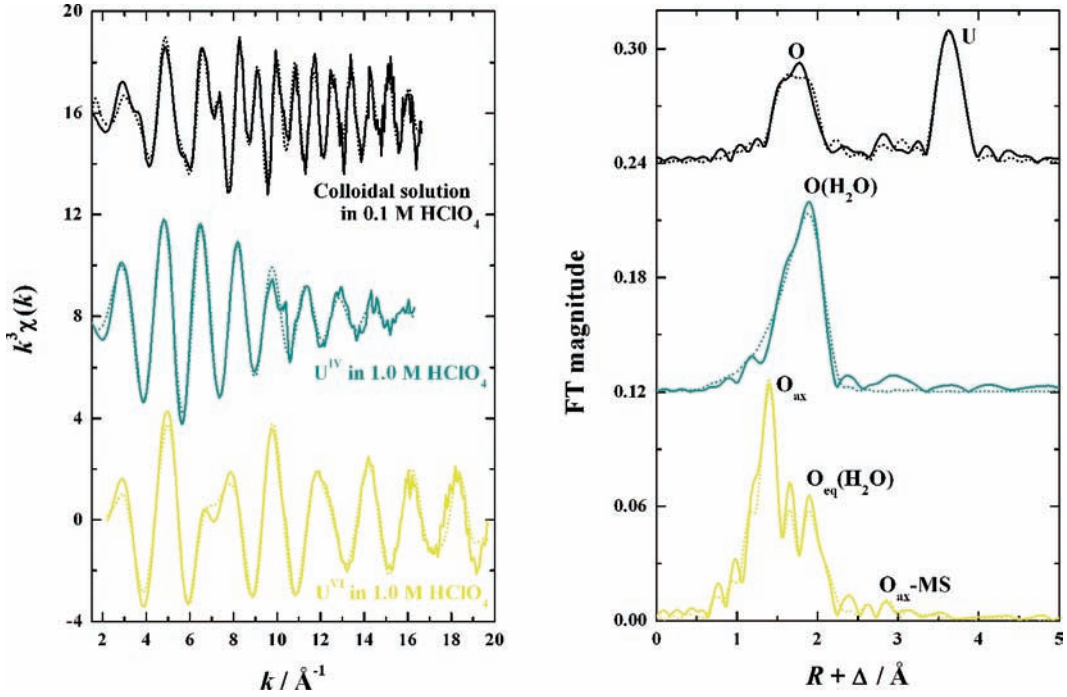

Figure 1. The k^3-weighted U L_{III}-edge EXAFS spectra of U^{IV} and U^{VI} samples in $HClO_4$ (left) and their corresponding Fourier transforms (right): solid lines (−), experimental data; dotted lines (···), theoretical fit; phase shifts (△) are not corrected on FTs. The data color reflects the actual color of sample solutions.

S_0^2 value of 0.9, while we get the CN of 9.5 when assuming the S_0^2 value of 1.0. Taking all these facts together, we conclude that the U^{IV} (and Np^{IV}) hydrate species possibly possess a CN of both 9 and 10, and hence, 9- and 10-coordinate hydrate complexes are probably coexisting in the actual solution. This is still consistent with the present EXAFS results within the error limit.

Contrary to the tetravalent state, there is a difference in structural parameters between the hexavalent An of U^{VI} and Np^{VI}. That is, Np^{VI} exhibits a shorter $R(An-O_{ax})$ of 1.76 Å and a longer $R(An-O_{eq}(H_2O))$ of 2.42 Å[18] than the corresponding interatomic distances for U^{VI}. Several DFT and MP2 studies[41] have predicted that both $An-O_{ax}$ and $An-O_{eq}(H_2O)$ distances in $[An^{VI}O_2(H_2O)_5]^{2+}$ shorten across U to Pu, being contradictory to the present EXAFS results. A recent DFT study by Tsushima[42] has indicated that the potential energy surfaces for the aquo complexes of $U^{VI}O_2^{2+}$ and $Np^{VI}O_2^{2+}$ show many local energy minima around their equilibrium geometries, potentially leaving uncertainty in the $An-O_{eq}(H_2O)$ distances. This problem comes from the fact that there is hitherto no appropriate method to search the Gibbs energy minimum in the present DFT calculations. At the moment, the common way to find the stable geometry is searching for the electronic energy minimum, although this is not necessarily equal to the Gibbs energy minimum. In addition, going across the An series increases the number of 5f electrons, making the 5f orbitals more contracted radially.[43] The role of 5f electrons in chemical bonding is still a matter of discussion even to date, and hence, further detailed investigation is required to give a clear explanation for the contradiction between the present EXAFS results and theoretical studies.

As shown in Figure 1, the black colloidal solution sample exhibits a completely different EXAFS oscillation pattern and FT, as compared to those for U^{IV} and U^{VI} in 1.0 M $HClO_4$. The pH of the colloidal solution was found to be slightly increased to 1.6 after the electrolysis. Since no hydrolysis product can occur in such a low pH region,[2] the colloid should be some oxide compounds. As a matter of fact, the observed EXAFS spectrum and FT are analogous to those observed for UO_2 compounds.[44] Therefore, the EXAFS curve fitting for the colloidal sample was performed by assuming the crystal structure of UO_2.[45] The obtained structural parameters are summarized in Table 1, along with those for the reported crystalline UO_2[44a,44b] and amorphous hydrous oxide $UO_2 \cdot nH_2O$.[44c] The EXAFS structural parameters calculated for the black colloidal solution are not similar to those reported for crystalline UO_2,[44a,44b] but the CN(U) = 6.0 for the colloidal solution is close to that for the reported $UO_2 \cdot nH_2O$ (6.3).[44c] These results indicate that the electroreduction of U^{VI} under lower acidic conditions (0.1 M $HClO_4$, in the present case) produces a colloidal

(41) (a) Hay, P. J.; Martin, R. L.; Schreckenbach, G. *J. Phys. Chem. A* **2000**, *104*, 6259–6270. (b) Shamov, G. A.; Schreckenbach, G. *J. Phys. Chem. A* **2005**, *109*, 10961–10974. (c) Tsushima, S.; Wahlgren, U.; Grenthe, I *J. Phys. Chem. A* **2006**, *110*, 9175–9182. (d) Steele, H.; Taylor, R. J. *Inorg. Chem.* **2007**, *46*, 6311–6318.

(42) Tsushima, S. *J. Phys. Chem. A* **2007**, *111*, 3613–3617.

(43) Kaltsoyannis, N.; Hay, P. J.; Li, J.; Blaudeau, J.-P.; Bursten, B. E. In *The Chemistry of the Actinide and Transactinide Elements*; Morss, L. R., Edelstein, N. M., Fuger, J., Eds.; Springer: Dordrecht, The Netherlands, 2006; *Vol. 3*, p 1923.

(44) (a) Conradson, S. D.; Manara, D.; Wastin, F.; Clark, D. L.; Lander, G. H.; Morales, L. A.; Rebizant, J.; Rondinella, V. V. *Inorg. Chem.* **2004**, *43*, 6922–6935. (b) Schofield, E. J.; Veeramani, H.; Sharp, J. O.; Suvorova, E.; Bernier-Latmani, R.; Mehta, A.; Stahlman, J.; Webb, S. M.; Clark, D. L.; Conradson, S. D.; Ilton, E. S.; Bargar, J. R. *Environ. Sci. Technol.* **2008**, *42*, 7898–7904. (c) Opel, K.; Weiβ, S.; Hübener, S.; Zänker, H.; Bernhard, G. *Radiochim. Acta* **2007**, *95*, 143–149.

(45) Loopstra, B. O. *Acta Crystallogr.* **1970**, *B26*, 656–657.

Table 1. Summary of EXAFS Structural Parameters and Results of DFT Calculations at the B3LYP Level in Aqueous Solution

		$O(H_2O)$		$O_{co}(NO_3)$		$N(NO_3)$		$O_{dist}(NO_3)$, MS[a]	
oxidation state of U	medium	CN[b]	R/Å[c]	CN[b]	R/Å[c]	CN[b]	R/Å[c]	CN[b]	R/Å[c]
IV	1.0 M $HClO_4$	10.5	2.40						
	1.3 M HNO_3	8.3	2.40	2.8	2.53	1.4	2.94	1.4	4.18
	2.6 M HNO_3	6.1	2.38	4.6	2.50	2.3	2.95	2.3	4.19
	3.9 M HNO_3	5.0	2.38	5.5	2.50	2.7	2.97	2.7	4.20
	5.2 M HNO_3	4.0	2.39	7.0	2.49	3.5	2.97	3.5	4.19
	6.4 M HNO_3	2.6	2.39	8.2	2.49	4.1	2.98	4.1	4.20
	7.7 M HNO_3	2.1	2.39	8.6	2.50	4.3	2.99	4.3	4.21
	9.0 M HNO_3	1.1	2.39	9.5	2.50	4.7	2.99	4.7	4.20

		O_1		O_2		O_3		O_4		U	
oxidation state of U	medium	CN[b]	R/Å[c]	CN[b]	R/Å[c]	CN[b]	R/Å[c]	CN[b]	R/Å[c]	CN[b]	R/Å[c]
IV (black colloid)	0.1 M $HClO_4$	2.0	1.94			4.2	2.37	2.3	2.52	6.0	3.82
	UO_2 (solid)[d]	0.6	1.94			7.6	2.36			10.6	3.88
IV	UO_2 (solid)[e]					8	2.35			12	3.87
	$UO_2 \cdot nH_2O$[f]					8.1	2.34			6.3	3.86

		O_{ax}		$O_{eq}(H_2O)$		$O_{eq\text{-}co}(NO_3)$		$N(NO_3)$		$O_{dist}(NO_3)$, MS[a]	
oxidation state of U	medium	CN[b,g]	R/Å[c]	CN[b]	R/Å[c]	CN[b]	R/Å[c]	CN[b]	R/Å[c]	CN[b]	R/Å[c]
VI	1.0 M $HClO_4$	2.0	1.77	5.0	2.40						
	2.9 M HNO_3	2.0	1.77	3.6	2.39	2.1	2.49	1.1	2.94	1.1	4.19
	5.8 M HNO_3	2.0	1.77	2.5	2.39	3.3	2.49	1.7	2.94	1.7	4.19
	8.7 M HNO_3	2.0	1.77	1.6	2.39	4.2	2.50	2.1	2.96	2.1	4.19
	11.6 M HNO_3	2.0	1.77	1.3	2.39	4.6	2.51	2.3	2.96	2.3	4.20
	14.5 M HNO_3	2.0	1.77	1.2	2.39	4.9	2.51	2.5	2.96	2.5	4.20

DFT-optimized complexes	R/Å	R/Å	R/Å	R/Å	R/Å	ID[h]
$[U^{VI}O_2(H_2O)_5]^{2+}$	1.76	2.44				A
$[U^{VI}O_2(H_2O)_4NO_3]^{+}$ (unidentate)	1.76	2.46	2.36	3.44	4.43	B
$[U^{VI}O_2(H_2O)_3NO_3]^{+}$ (bidentate)	1.76	2.41	2.49	2.95	4.16	C
$[U^{VI}O_2H_2O(NO_3)_2]^{0}$ (CN = 5)	1.76	2.39	2.47	2.93	4.14	D
$[U^{VI}O_2(H_2O)_2(NO_3)_2]^{0}$ (CN = 6)	1.76	2.49	2.51	2.97	4.19	E
$[U^{VI}O_2(NO_3)_3]^{-}$	1.76		2.50	2.96	4.18	F
$[U^{VI}O_2(NO_3)_4]^{2-}$	1.76		2.43(uni)/2.56(bi)	3.45(uni)/3.02(bi)	4.57(uni)/4.25(bi)	G

[a] MS: multiple scattering paths corresponding to the linear U−N−O_{dist} arrangement. [b] Error: CN ≤ ±10%. [c] Error: R ≤ ±0.01 Å. [d] Reported values in ref 44a. [e] Reported values in ref 44b. [f] Reported values in ref 44c. [g] Fixed values. [h] Corresponding IDs in Figure 7.

$U^{IV}O_2 \cdot nH_2O$. The structure of this oxide compound is most likely to be distorted due to the presence of water molecules inside the basic UO_2 framework, giving a shorter U−U distance and lower CN(U) as compared to those for crystalline UO_2.

U(IV) in Nitric Acid System. U^{IV}−nitrate samples were prepared by the electroreduction of U^{VI} solutions with different HNO_3 concentrations using a Pt working electrode. The electrolysis in more than 10 M HNO_3 merely resulted in H_2 gas production on working and counter electrodes, and no reduction from U^{VI} to U^{IV} occurred even after several hours. As a consequence, the HNO_3 concentration in U^{IV}−nitrate samples could be varied from 0 to 9 M. UV−visible−NIR absorption spectra of the prepared U^{IV}−nitrate solution samples are shown in Figure 2. As previously reported,[3] the absorption spectra of U^{IV} are changed with an increase in HNO_3 concentration, implying that U^{4+} forms a complex with NO_3^- even at the lowest HNO_3 concentration of 1.3 M.

Figure 3 shows the k^3-weighted EXAFS spectra for the U^{IV}−nitrate solutions (left) and their corresponding FTs (right), along with those for U^{IV} in 1.0 M $HClO_4$ as a reference (i.e., [HNO_3] = 0 M). EXAFS oscillation patterns are gradually changed with increasing HNO_3 concentration, especially in the k range over 7 $Å^{-1}$.

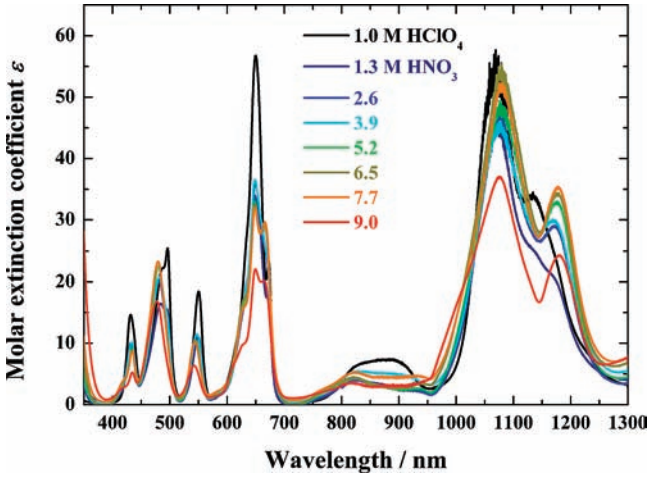

Figure 2. UV−visible−NIR absorption spectra of U^{IV} at different HNO_3 concentrations: [U] = 0.05 M.

Their FTs display a systematic change with the increase in HNO_3 concentration. That is, as illustrated more clearly in Figure 4, the largest peak at $R + \Delta = 1.9$ Å becomes smaller and shifts to a higher R range. In addition, two more distinguishable peaks grow larger at around

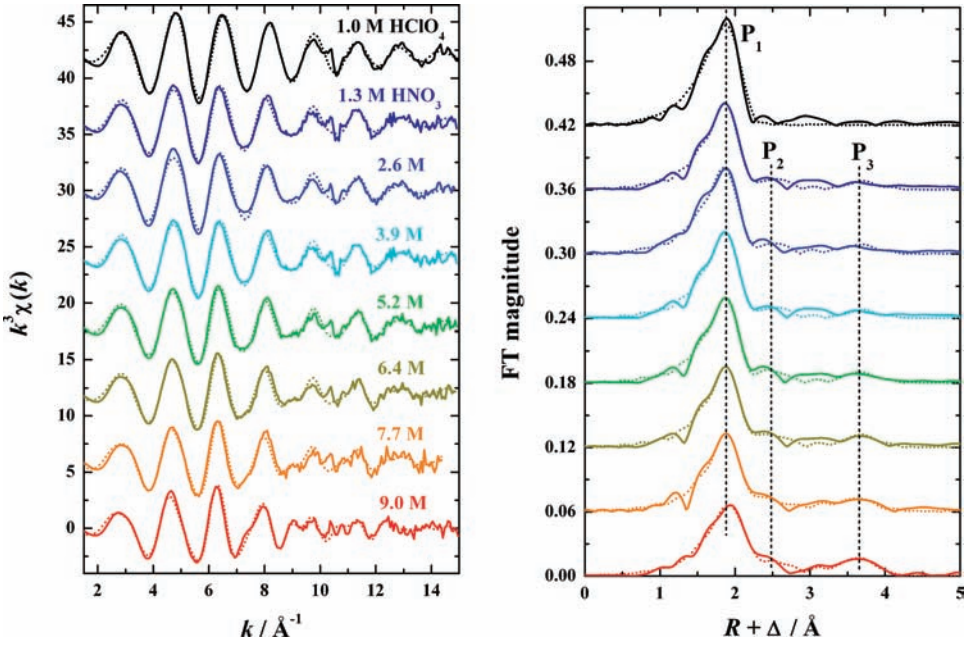

Figure 3. The k^3-weighted U L_{III}-edge EXAFS spectra of U^{IV} at different HNO_3 concentrations (left) and their corresponding Fourier transforms (right): solid lines (−), experimental data; dotted lines (···), theoretical fit; phase shifts (Δ) are not corrected on FTs. P_1, SS of $O(H_2O)$ and $O_{co}(NO_3)$; P_2, SS of $N(NO_3)$; P_3, SS of $O_{dist}(NO_3)$ and MS of NO_3^-.

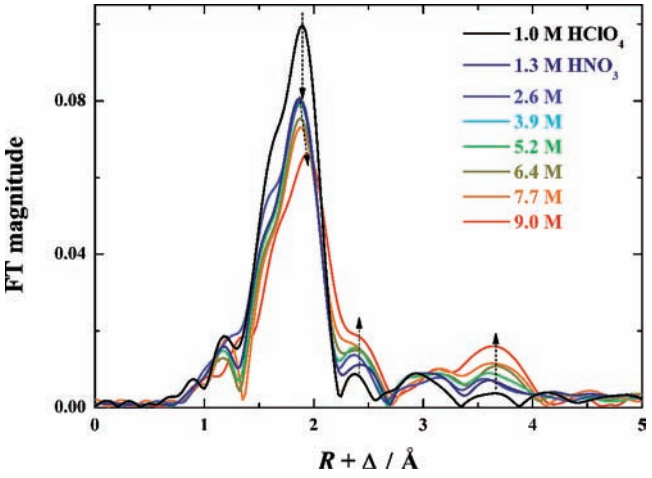

Figure 4. Comparison of Fourier transforms for the EXAFS data of U^{IV} at different HNO_3 concentrations: FT range, k = 1.5−14.5 $Å^{-1}$; phase shifts (Δ) are not corrected.

$R + \Delta = 2.5$ and 3.6 Å. Similar systematic changes have been observed in the EXAFS spectra for Np^{IV}−[18] and Pu^{IV}−HNO_3[19] systems, in which An^{4+} is coordinated by NO_3^- in a planar bidentate mode. As a matter of fact, the relative distances between the first (P_1) and second peaks (P_2) and between the second (P_2) and third (P_3) peaks in Figure 3 are well-consistent with the arrangement for the planar bidentate coordination,[13,14,18,19,46] as illustrated in Figure S3 in the Supporting Information, rather than that for the unidentate one. Taken together, it is reasonable to conclude that the planar bidentate geometry is dominant for the complexation between U^{4+} and NO_3^-, and hence, the obtained spectra were analyzed on the assumption that NO_3^- is coordinated in the bidentate fashion.

The EXAFS structural parameters obtained from the curve fitting are summarized in Table 1. As expected from the FTs in Figure 4, systematic changes are found for the CNs of water molecules ($O(H_2O)$), nitrate oxygens directly coordinating to U ($O_{co}(NO_3)$), nitrogens of NO_3^- ($N(NO_3)$), and distal oxygens of NO_3^- ($O_{dist}(NO_3)$), as a function of HNO_3 concentration. That is, $CN(O(H_2O))$ decreases gradually, while the CNs related to coordinating NO_3^- (i.e., $CN(O_{co}(NO_3))$, $CN(N(NO_3))$, and $CN(O_{dist}(NO_3))$) increase proportionally, with increasing HNO_3 concentration. This indicates that hydrate water molecules are replaced by bidentate-coordinating NO_3^- successively with the increase in HNO_3 concentration. Thermodynamic data[2] suggest the presence of four fundamental U^{IV}−nitrate species from U/NO_3 = 1:1 to 1:4 in aqueous solution. The speciation distribution profile estimated from the reported formation constants between U^{4+} and NO_3^- in aqueous solution[2] is given in Figure S15 in the Supporting Information. Assuming that the speciation of the U^{IV}−nitrate system is terminated with the formation of the tetranitrato complex and the fifth U^{IV}−nitrate species of the pentanitrato complex is not formed, the speciation change is expected to be saturated with the tetranitrate species (i.e. $CN(NO_3) = 4$) at around 5 M HNO_3, as shown in Figure S15 (Supporting Information). However, a considerable change is observed both in the UV−visible−NIR (Figure 2) and in the EXAFS spectra (Figure 4), even between 7.7 and 9.0 M HNO_3 samples. This indicates that the speciation is still changing in the higher HNO_3 concentration range above 5 M. It is well-known that An^{4+}, including U^{4+}, are strongly adsorbed on anion exchangers in the HNO_3 system,[47] in which

(46) Gaillard, C.; Chaumont, A.; Billard, I.; Hennig, C.; Ouadi, A.; Wipff, G. *Inorg. Chem.* **2007**, *46*, 4815–4826.

(47) (a) Ryan, J. L.; Wheelwright, E. *J. Ind. Eng. Chem.* **1959**, *51*, 60–65. (b) Navratil, J. D.; Wei, Y. *Nukleonika* **2001**, *46*, 75–80. (c) Wei, Y.; Arai, T.; Hoshi, H.; Kumagai, M.; Bruggeman, A.; Goethals, P. *Nucl. Technol.* **2005**, *149*, 217–231.

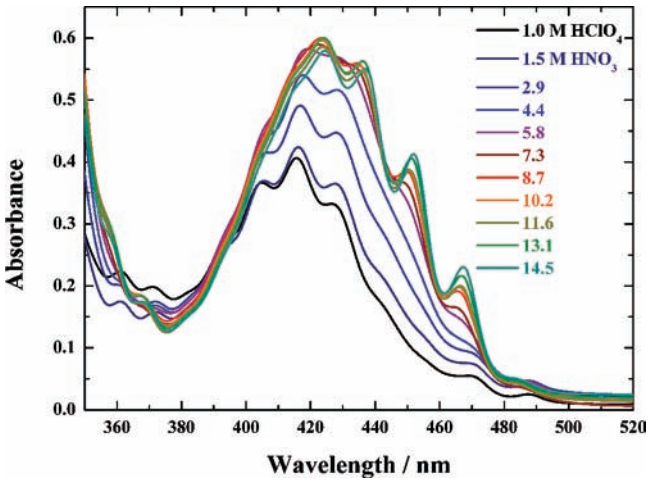

Figure 5. UV−visible absorption spectra of 0.04 M U^{VI} at different HNO_3 concentrations: optical path length, 1.00 cm.

these tetravalent cations interact with anion exchange functional sites as negatively charged nitrato complexes, such as $[An^{IV}(H_2O)_m(NO_3)_5]^-$ or $[An^{IV}(H_2O)_n(NO_3)_6]^{2-}$. Additionally, several X-ray absorption studies[19,48] have proposed the presence of the hexanitrato Pu^{IV} complex, $[Pu^{IV}(NO_3)_6]^{2-}$, in concentrated HNO_3. Considering these facts, we conclude that U^{4+} forms negatively charged nitrato complexes, such as $[U^{IV}(H_2O)_x(NO_3)_5]^-$ or $[U^{IV}(H_2O)_y(NO_3)_6]^{2-}$, at a higher HNO_3 concentration range. Although we cannot judge whether the $CN(NO_3)$ ($= CN(O_{co}(NO_3))/2 = CN(N(NO_3))$) of 4.7 obtained for the 9.0 M HNO_3 sample is the average of tetra- and pentanitrate species or the average of tetra-, penta-, and hexanitrate species, the present EXAFS results suggest that the pentanitrato complex, $[U^{IV}(H_2O)_x(NO_3)_5]^-$, is the most dominant species in 9.0 M HNO_3. The calculated interatomic distances between U^{IV} and $O_{co}(NO_3)$ (2.49−2.53 Å) and between U^{IV} and $N(NO_3)$ (2.95−2.99 Å) are close to those reported for Np^{IV} [$R(O_{co}(NO_3)) = 2.51-2.52$ Å and $R(N(NO_3)) = 2.96$ Å][18] and Pu^{IV} [$R(O_{co}(NO_3)) = 2.49$ Å and $R(N(NO_3)) = 2.97$ Å][19] but much shorter than that for Th^{IV} [$R(O_{co}(NO_3)) = 2.63$ Å].[49] This difference in the interatomic distances between U^{IV} and Th^{IV} is larger than the difference in their ionic radii, probably indicating that the nitrate coordination for U^{4+} is stronger than that for Th^{4+} but similar to those for Np^{4+} and Pu^{4+}. It should be noted that there is an increasing tendency for $R(N(NO_3)$ with the increase in HNO_3 concentration, although $R(O_{co}(NO_3))$ is almost constant regardless of HNO_3 concentration. This might suggest that the $O_{co}1-N-O_{co}2$ angle of coordinating NO_3^- (illustrated in Figure S3 in the Supporting Information) becomes narrower with increasing HNO_3 concentration. The total CN of the U^{4+} primary coordination sphere ($= CN(O(H_2O)) + CN(O_{co}(NO_3))$) is relatively settled and fluctuates between 10.5 and 11.1, regardless of the HNO_3 concentration.

U(VI) in Nitric Acid System. Figure 5 shows the UV−visible absorption spectra of U^{VI} at different HNO_3 concentrations. The absorbance of the main absorption band for U(VI) from 375 to 500 nm[50] gradually increases with an increase in the HNO_3 concentration. In addition, the spectral shape becomes dull at first, and then clear absorption peaks rise gradually at around 423, 436, 452, and 467 nm with the increase in HNO_3 concentration. This variation tendency is well-consistent with the previously reported results for the same $U^{VI}-HNO_3$ system.[12] These spectra were analyzed on the nonlinear least-squares regression program *Hyperquad*[51] to estimate the number of fundamental species in the system by defining the following chemical equilibrium:

$$UO_2^{2+} + nNO_3^- \leftrightarrow [UO_2(NO_3)_n]^{2-n}$$

The fitting results suggest that there are four fundamental species in the system, that is, pure hydrate and mono-, di-, and trinitrate species.

Subsequently, EXAFS measurements were carried out using the same solution samples employed for the above UV−visible absorption measurement. The collected EXAFS spectra (k^3-weighted, left) and their corresponding FTs (right) are given in Figure 6. Clear EXAFS oscillation patterns are observed until $k = 19.5$ Å^{-1} for all of the samples, giving a distance resolution, ΔR ($= \pi/2\Delta k$), of 0.09 Å. The obtained FTs indicate that the peak at $R + \Delta = 1.9$ Å (P_2), which corresponds to the SS path of $O_{eq}(H_2O)$, becomes smaller with increasing HNO_3 concentration. Instead, three additional peaks grow larger at $R + \Delta = 2.1$ (P_3), 2.6 (P_4), and 3.8 Å (P_5). It is obvious from the discussion in the U(IV) section and reported studies[13,14,46] that these peaks are attributed to be the SS paths for the coordinating oxygens and nitrogens of NO_3^- ($O_{eq-co}(NO_3)$), $N(NO_3)$, $O_{dist}(NO_3)$, and its MS paths, respectively. The distance difference between these three scattering shells are, again, well-consistent with a planar bidentate coordination fashion, rather than the unidentate one. These characteristic peaks clearly demonstrate the presence of inner sphere coordination of nitrate ions with the bidentate mode, and thus, they were used to determine the average CN of bidentate coordinate NO_3^- ($CN(bi\text{-}NO_3)$). The superposition of P_1 and P_2 produces an additional FT peak between them ($R + \Delta = 1.6-1.7$ Å), although it is chemically meaningless.[18]

It should be noted that the obtained EXAFS spectra always represent a mixture of several fundamental species, and hence, analyzing these spectra provides no direct information about each individual species. However, we can estimate the average $CN(bi\text{-}NO_3)$ from the above-mentioned characteristic FT peaks of P_3, P_4, and P_5 in Figure 6. The obtained EXAFS structural parameters are summarized in Table 1. As confirmed in the perchloric acid section, U^{VI} exists as a uranyl ion (UO_2^{2+}) with five

(48) Conradson, S. D.; Abney, K. D.; Begg, B. D.; Brady, E. D.; Clark, D. L.; den Auwer, C.; Ding, M.; Dorhout, P. K.; Espinosa-Faller, F. J.; Gordon, P. L.; Haire, R. G.; Hess, N. J.; Hess, R. F.; Keogh, D. W.; Lander, G. H.; Lupinetti, A. J.; Morales, L. A.; Neu, M. P.; Palmer, P. D.; Paviet-Hartmann, P.; Reilly, S. D.; Runde, W. H.; Tait, C. D.; Veirs, D. K.; Wastin, F. *Inorg. Chem.* **2004**, *43*, 116–131.

(49) Johansson, G.; Magini, M.; Ohtaki, H. *J. Solution Chem.* **1991**, *20*, 775–792.

(50) Rabinowitch, E.; Belford, R. L. *Spectroscopy and Photochemistry of Uranyl Compounds*; Pergamon Press: London, 1964.

(51) Gans, P.; Sabatini, A.; Vecca, A. *Talanta* **1996**, *43*, 1739–1753.

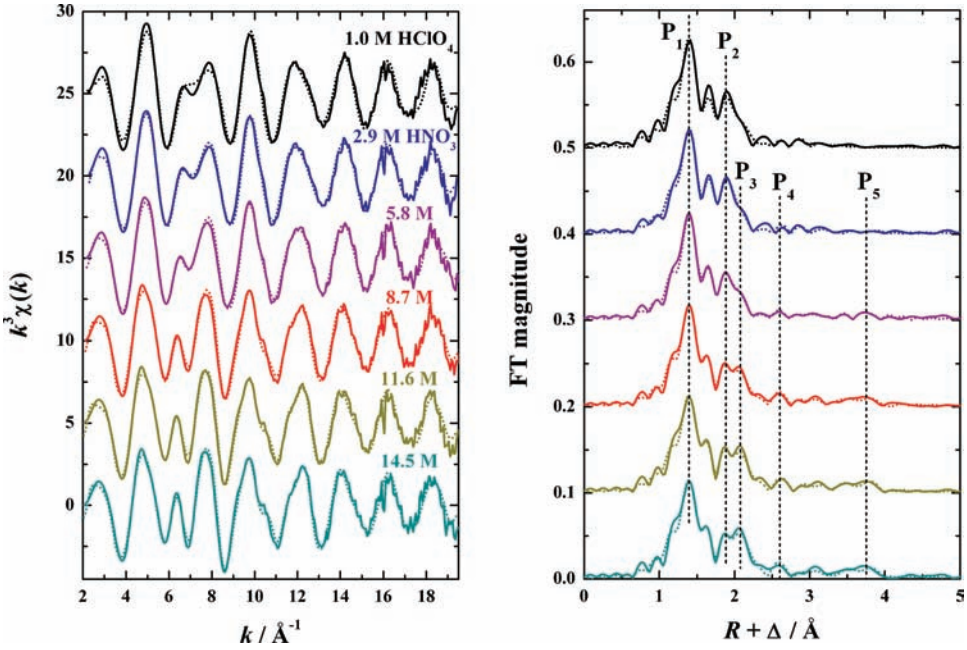

Figure 6. The k^3-weighted U L_{III}-edge EXAFS spectra of U^{VI} at different HNO_3 concentrations (left) and their corresponding Fourier transforms (right): solid lines (−), experimental data; dotted lines (···), theoretical fit; phase shifts (△) are not corrected on FTs. P1, SS of O_{ax}; P_2, SS of $O_{eq}(H_2O)$; P_3, SS of $O_{eq-co}(NO_3)$; P_4, SS of $N(NO_3)$; P_5, SS of $O_{dist}(NO_3)$ and MS of NO_3^-.

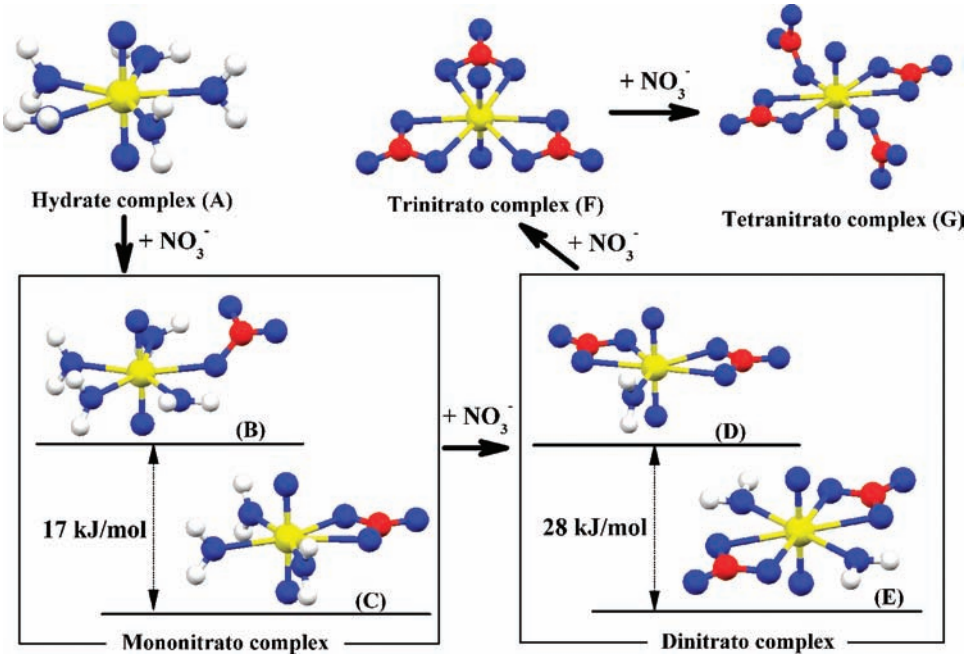

Figure 7. DFT-optimized structures for pure hydrate and mono-, di-, tri-, and tetranitrato complexes of U^{VI} at the B3LYP level in aqueous solution. Calculated bond distances are given in Table 1; an additional water molecule (not shown) was placed in the outer coordination spheres of structures **C** and **D** in order to make the corresponding two complexes (i.e., structures **B** and **C** and structures **D** and **E**) comparable in energy.

water molecules on its equatorial plane in the absence of NO_3^- (i.e., 0 M HNO_3 = 1.0 M $HClO_4$ in Figure 6), forming a 5-fold hydrate complex of $[U^{VI}O_2(H_2O)_5]^{2+}$. This is consistent with the previously reported NMR,[52,53] X-ray diffreaction,[52] and EXAFS[54] results and DFT calculations.[42] The present EXAFS results suggest that $CN(H_2O)$ (= $CN(O_{eq}(H_2O))$ gradually decreases and, to the contrary, $CN(bi\text{-}NO_3)$ increases with increasing HNO_3 concentration. As compared with the pure hydrate species, the $U-O_{eq}(H_2O)$ distance becomes shorter at a lower HNO_3 concentration range (≤5.8 M), while it lengthens at a higher HNO_3 concentration range (≥8.7 M). On the other hand, the $U-O_{eq}(bi-NO_3)$ and U−N distances become longer by degrees with the increase in HNO_3

(52) Åberg, M.; Ferri, D.; Glaser, J.; Grenthe, I. *Inorg. Chem.* **1983**, *22*, 3986–3989.
(53) Bardin, N.; Rubini, P.; Madic, C. *Radiochim. Acta* **1998**, *83*, 189–194.
(54) (a) Allen, P. G.; Bucher, J. J.; Shuh, D. K.; Edelstein, N. M.; Reich, T. *Inorg. Chem.* **1997**, *36*, 4676–4683. (b) Hennig, C.; Schmeide, K.; Brendler, V.; Moll, H.; Tsushima, S.; Scheinost, A. C. *Inorg. Chem.* **2007**, *46*, 5882–5892.

concentration. Although the reported crystal structures for uranyl nitrate hydrate compounds show somewhat scattered values, the interatomic distances calculated for the aqueous $U^{VI}-NO_3^-$ species are in agreement with those observed in the crystal structure (i.e., $R(U-O_{ax}) = 1.74-1.76$ Å, $R(U-O_{eq}(H_2O)) = 2.40-2.45$ Å, and $R(U-O_{eq}(bi-NO_3) = 2.49-2.54$ Å, respectively).[28,55]

Although the present EXAFS results provide no direct information about the spatial arrangement of individual species, we can presume their possible structures from the EXAFS results with the help of DFT calculations. As already discussed above, it is clear that the pure hydrate species corresponds to $[U^{VI}O_2(H_2O)_5]^{2+}$ with an equatorial coordination number (CN_{eq}) of 5. The trinitrate species probably forms a 6-fold bidentate coordinate trinitrato complex of $[U^{VI}O_2(NO_3)_3]^-$, as has been found both in a solid state[55a] and in a solution state.[13,14] This indicates that the CN_{eq} increases from 5 to 6 with increasing NO_3^- coordination. On the other hand, determining the structural arrangement of the mono- and dinitrate species is not straightforward, and several different structures are conceivable. To the best of our knowledge, the reported crystals of uranyl dinitrato hydrate complexes exhibit a bidentate fasion for the NO_3^- coordination and never show the unidentate one (e.g., refs 28, 55b, and 55c). Furthermore, a recent molecular dynamics (MD) study by Bühl et al.[16] has suggested that the bidentate fashion is more favorable for the dinitrate complex than the unidentate one in aqueous solution. Therefore, the dinitrate species in the present HNO_3 system is likely to possess bidentate coordinate NO_3^-. Since the bidentate dinitrate species may form 5- or 6-fold complexes, the DFT calculations have been performed for a 5-fold dinitrato monohydrate complex, $[U^{VI}O_2(H_2O)(NO_3)_2]^0$ (structure **D** in Figure 7) and a 6-fold dinitrato dihydrate complex, $[U^{VI}O_2(H_2O)_2(NO_3)_2]^0$ (D_{2h}, structure **E** in Figure 7). The results suggest that the 6-fold complex is 28.0 kJ/mol more stable in Gibbs free energy than the 5-fold one. Taken together, the 6-fold bidentate coordinate dinitrato complex is regarded as the most probable structure for the dinitrate species. The average interatomic distances for the DFT-optimized complexes are summarized in Table 1. The mononitrate species also has several possibilities for its structural arrangement. So far, no crystal structure has been reported for the uranyl mononitrato hydrate complex. However, U^{VI} can form mononitrato complexes with organic ligands, displaying a unidentate fashion (e.g., ref 56). Another MD study by Bühl et al.[17] has proposed that the 6-fold mononitrato complex is less stable than the 5-fold one in aqueous solution, whereas there is almost no difference in free energy between the unidentate and bidentate coordination modes for the 5-fold complexes. This MD study by Bühl et al. employed the BLYP functional with large core ECP, while our calculations use the B3LYP functional with small core ECP, since Shamov and Schreckenbach have argued that the use of small core ECP is essential for getting accurate energy.[41b] Our DFT calculations at the B3LYP level suggest that a bidentate coordinate mononitrato trihydrate complex, $[U^{VI}O_2(H_2O)_3(\eta_2\text{-}NO_3)]^+$ ($CN_{eq} = 5$, structure **C** in Figure 7 and called "η_2-complex" hereafter), is slightly more stable (−17.0 kJ/mol) in aqueous solution than a unidentate coordinate mononitrato tetrahydrate complex, $[U^{VI}O_2(H_2O)_4(\eta_1\text{-}NO_3)]^+$ ($CN_{eq} = 5$, structure **B** in Figure 7 and called "η_1-complex", hereafter). In addition, it has been reported that the η_2-complex is dominant for the mononitrate species also in acetonitrile, rather than the η_1-complex.[14] Considering these facts, we conclude that the η_2-complex is more probable for the mononitrate species in aqueous solution. One may expect the presence of a tetranitrate species in a higher HNO_3 concentration range. As illustrated in the upper right of Figure 7, the DFT-optimized tetranitrato U^{VI} complex has two unidentate coordinate NO_3 and two bidentate coordinate NO_3 on its equatorial plane with $CN_{eq} = 6$, agreeing with the reported MD study.[17] The $U-N(\eta_1\text{-}NO_3)$ and $U-O_{dist}(\eta_1\text{-}NO_3)$ distances in the optimized tetranitrato complex are calculated to be much longer than the $U-N(\eta_2\text{-}NO_3)$ and $U-O_{dist}(\eta_2\text{-}NO_3)$ distances. This means that, when we assume the presence of the tetranitrate species in the present HNO_3 system, the observed $U-N(NO_3)$ and $U-O_{dist}(NO_3)$ distances should lengthen with increasing HNO_3 concentration, as a result of the formation of the tetranitrato complex at a higher HNO_3 concentration range. This is, however, inconsistent with the EXAFS results shown in Figure 6 and the calculated structural parameters: the $U-N(NO_3)$ and $U-O_{dist}(NO_3)$ distances are almost constant with the appropriate values for bidentate coordinate NO_3^- even at a higher HNO_3 concentration. In addition, the UV−visible spectral analysis assuming the presence of the tetranitrate species never converged, and no reasonable results were obtained. These results suggest that the tetranitrate species is not formed (or formed at an inconsiderable amount), and hence, the $U^{VI}-NO_3^-$ complexation system in HNO_3 terminates with the formation of the trinitrate species. Note that the present DFT calculations do not simulate actual speciation perfectly, because the obtained energy difference represents the values at the zero ionic strength. This indicates that the calculated speciation might differ from the actual speciation, especially at higher ionic strength conditions. Despite this fact, the importance of theoretical calculations on the speciation study should be still emphasized to estimate the possible coordination geometry of each chemical species.

Conclusions

The present multitechnique study employing UV−visible−NIR and EXAFS spectroscopies and DFT calculations has revealed the speciation and complex structure of the aquo nitrate species of U^{IV} and U^{VI} in aqueous acidic solutions of $HClO_4$ and HNO_3. U^{IV} exists as a spherical tetravalent cation (U^{4+}) and forms a nona- or decahydrate complex, $[U^{IV}(H_2O)_{9-10}]^{4+}$, as a dominant species in 1.0 M $HClO_4$, while it forms a colloidal compound of $U^{IV}O_2 \cdot nH_2O$ at a lower acid concentration of 0.1 M $HClO_4$. In the HNO_3 system, the hydrate water molecules in the primary coordination sphere

(55) (a) Zalkin, A.; Templeton, L. K.; Templeton, D. H. *Acta Crystallogr.* **1989**, *C45*, 810–811. (b) Hughes, K.-A.; Burns, P. C. *Acta Crystallogr.* **2003**, *C59*, i7–i8. (c) Shuvalov, R. R.; Burns, P. C. *Acta Crystallogr.* **2003**, *C59*, i71–i73.

(56) (a) Bandoli, G.; Clemente, D. A.; Cingi, M. B. *J. Inorg. Nucl. Chem.* **1975**, *37*, 1709–1714. (b) Graziani, R.; Marangoni, G.; Paolucci, G.; Forsellini, E. *J. Chem. Soc., Dalton Trans.* **1978**, 818–826.

of U^{IV} are replaced successively by planar bidentate coordinate NO_3^-, finally forming a pentanitrato complex, $[U^{IV}(H_2O)_x(NO_3)_5]^-$, as a dominant species in 9.0 M HNO_3. On the other hand, U^{VI} exists as a transdioxo cation, UO_2^{2+}, and possesses five water molecules on its equatorial plane to form a pure hydrate complex, $[U^{VI}O_2(H_2O)_5]^{2+}$, in 1.0 M $HClO_4$. The hydrate water molecules on the equatorial plane of UO_2^{2+} are also replaced by the bidentate coordinate NO_3^- as a function of increasing HNO_3 concentration. The $U^{VI}-NO_3^-$ complexation system in HNO_3 undergoes the formation of a 5-fold bidentate coordinate mononitrato complex, $[U^{VI}O_2(H_2O)_3(\eta_2\text{-}NO_3)]^+$, and a 6-fold bidentate coordinate dinitrato complex, $[U^{VI}O_2(H_2O)_2(\eta_2\text{-}NO_3)_2]^0$, with increasing HNO_3 concentration, terminating with the formation of a bidentate coordinate trinitrato complex, $[U^{VI}O_2(NO_3)_3]^-$. The presence of unidentate coordinate complexes or a tetranitrato U^{VI} complex is less probable in the present HNO_3 system.

Acknowledgment. We thank Y. Ikeda and K. Takao for the fruitful discussion on electrochemistry. This work was supported by the Deutsche Forschungsgemeinschaft under Contract HE2297/2-1. All of the DFT calculations in this study were performed on the supercomputer at Zentrum für Informationsdienste und Hochleistungsrechnen (ZIH), Technische Universität Dresden (TUD), Germany.

Supporting Information Available: CVs of U^{VI} in 1.0 M $HClO_4$; UV−visible−NIR absorption spectra that are not shown in the text; speciation distribution profile of $U^{IV}-NO_3^-$ species in HNO_3; schematic of the coordination geometry of a planar bidentate coordinate NO_3^-; detailed XANES and EXAFS spectra; calculated EXAFS structural parameters; EXAFS structural comparison among Th(IV), U(IV), and Np(IV); and coordinates for the DFT-optimized U^{VI} complexes. This material is available free of charge via the Internet at http://pubs.acs.org.